



ORIGINAL ARTICLE

# Rapid Fabrication of Silica Microlens Arrays via Glass 3D Printing

Chunxin Liu,<sup>1,2</sup> Taras Oriekhov,<sup>1,2</sup> Cherrie Lee,<sup>1</sup> Clarissa M. Harvey,<sup>1</sup> and Michael Fokine<sup>1,2</sup>

## Abstract

Rapid manufacturing of high purity fused silica glass micro-optics using a filament-based glass 3D printer has been demonstrated. A multilayer  $5 \times 5$  microlens array was printed and subsequently characterized, showing fully dense lenses with uniform focal lengths and good imaging performance. A surface roughness on the order of  $R_a = 0.12$  nm was achieved. Printing time for each lens was  $< 10$  s. Creating arrays with multifocal imaging capabilities was possible by individually varying the number of printed layers and radius for each lens, effectively changing the lens height and curvature. Glass 3D printing is shown in this study to be a versatile approach for fabricating silica micro-optics suitable for rapid prototyping or manufacturing.

**Keywords:** glass 3D printing, microlens, microlens array, freeform optics, laser processing

## Introduction

WITH THE DEVELOPMENT and miniaturization of modern optical systems, there is an increasing demand for small, complex, and tailored optical components. In recent years, the number of systems using microlenses or microlens arrays (MLAs), having micron to submillimeter dimensions, has increased due to their compact footprint, low weight, and improved optical performance.<sup>1</sup> The type of materials used for the fabrication of MLAs is limited and the choice depends on the specific application and optical requirements. For applications in the visible region, polymers are commonly used due to the benefits associated with low cost and the relative ease of processing and manufacturing.<sup>2,3</sup>

In more harsh conditions, high-performance materials may be required, for example, having properties such as increased thermal, chemical, or mechanical stability. For applications using light in the ultraviolet wavelength region, polymers have limitations due to their increased optical absorption. For many applications, the ideal material would be fused silica having an optical transmission window between  $\sim 180$  nm to  $2.5 \mu\text{m}$ . Silica glasses are well known for their high mechanical strength as well as their superior thermal and chemical stability.<sup>4</sup> However, these properties also come at a cost. Silica glass is hard and brittle and, therefore, difficult to

machine. With a softening point as high as  $1700^\circ\text{C}$ , thermal processing such as molding or embossing is extremely challenging. For chemical processing (etching), hydrofluoric acid is typically required.

Techniques used for fabricating glass MLAs include surface reshaping, and subtractive or additive manufacturing. The surface reshaping techniques include, for example, glass molding<sup>5</sup> and hot embossing.<sup>6</sup> These are suitable for high volume production, but generally suffer from high surface roughness ( $R_a < 120$  nm) and are applicable to multicomponent glasses with lower softening temperatures, such as soda lime<sup>4</sup> and borosilicate glass.<sup>5</sup> For small-scale production or prototyping these techniques are less attractive due to the high costs associated with making the mold or the master copy.

Subtractive manufacturing, in contrast, is more suitable for limited production and prototyping. This includes techniques ranging from, for example, wet<sup>7,8</sup> and reactive ion etching<sup>9–11</sup> to direct laser writing.<sup>12,13</sup> Novel approaches for producing glass MLAs involve structuring using femtosecond laser ablation with a subsequent surface smoothing using a carbon dioxide ( $\text{CO}_2$ ) laser.<sup>14–16</sup> Laser-induced wet etching,<sup>17</sup> black-body heating,<sup>18</sup> or backside dry etching have also been used.<sup>19</sup> The application of high power/pulsed lasers or chemical etching enables effective processing of high-grade optical glass such as fused quartz or fused silica.

<sup>1</sup>Department of Applied Physics, KTH Royal Institute of Technology, Stockholm, Sweden.

<sup>2</sup>Nobula3D AB, Stockholm, Sweden.

The submicron processing resolution of these techniques enables the formation of optically smooth surfaces ( $R_a \leq 100$  nm) on as-produced microlenses.<sup>7–19</sup> Using the aforementioned techniques, MLAs can be fabricated with highly customized optical characteristics and lens densities, with the size of microlenses ranging from a few microns to millimeters. Although highly applicable for scientific studies and prototyping, the subtractive nature of these technologies limits the application area to a small production volume due to the time-consuming production and the high cost.

Glass additive manufacturing is an emerging research topic showing an increase in publications in recent years.<sup>20–28</sup> Recent studies demonstrated MLA fabrication in fused silica using two-photon polymerization through a direct laser writing technique,<sup>29,30</sup> an approach that combined hot embossing with custom glass 3D printing,<sup>31</sup> stereolithography,<sup>32</sup> and microscale computed axial lithography.<sup>33</sup> These studies were realized by utilizing a new type of silica nanocomposite resin. After printing, thermal postprocessing is required to create fully dense glass microlenses. This includes removing the binder (polymer), followed by a high-temperature sintering step. This postprocessing can be time consuming, requiring several hours of heating. The debinding and sintering steps also result in significant volume shrink-

age, which can deform the structure and influence the resulting surface roughness of the print. Despite this challenge, the state-of-the-art techniques demonstrate up to 6 nm roughness for the printed surface after sintering.<sup>29,30,32,33</sup>

In this study, we report on 3D printing fused silica glass MLA through CO<sub>2</sub> laser heating of glass filaments. This technique enables highly customizable MLA design having sub-mm lens diameters, without the need for any thermal postprocessing. Through laser heating, lenses with sub-nm surface roughness can be achieved. The demonstrated technique is well suited for rapid prototyping of MLAs, as well as for small- to medium-size production in glass.

### Material and Fabrication

The feedstock material used for MLA fabrication was fused silica glass filaments, having a diameter of 200  $\mu$ m. The filaments were made using a conventional draw tower designed for optical fiber fabrication. Fused silica is a synthetic silicon dioxide glass of high purity, providing enhanced optical transmission in the wavelength range from  $\sim 180$  nm to 2.5  $\mu$ m, enabling MLAs to be designed for a large range of wavelengths. The MLA was fabricated directly onto a 25  $\times$  25 mm<sup>2</sup> fused quartz plate having a thickness of 300  $\mu$ m. A glass 3D printer (Nobula<sup>TM</sup> Zero; Nobula3D AB) was used

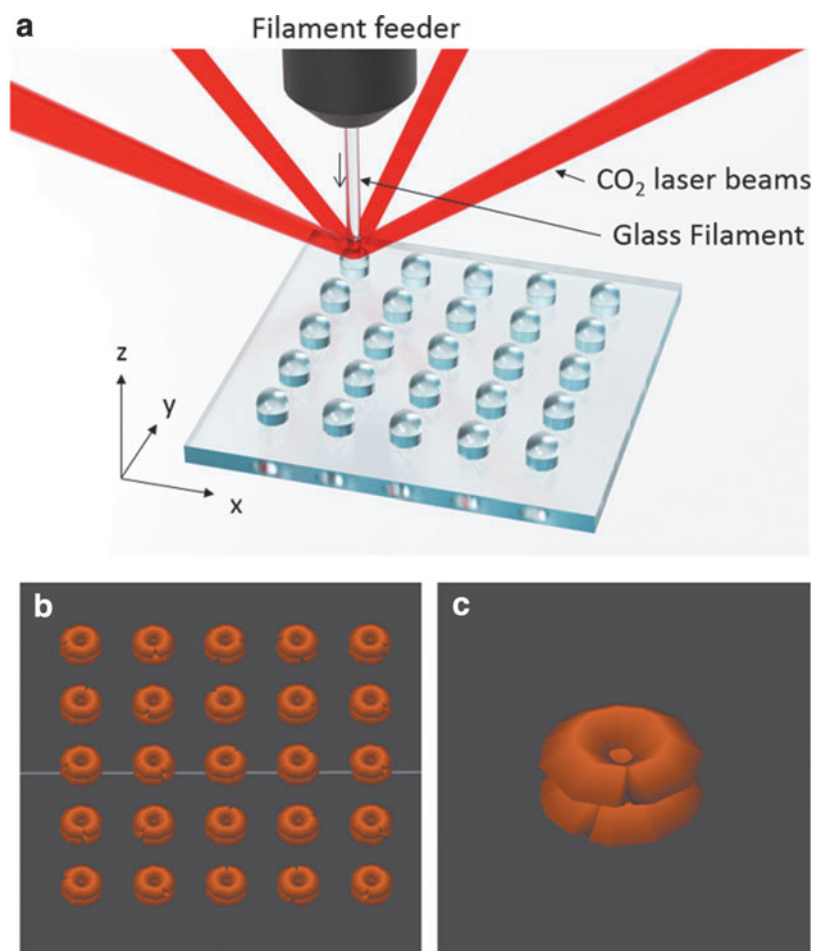


FIG. 1. (a) Schematic of process showing filament feeder and 4  $\times$  laser beams, (b) printing review of the MLA model, and (c) a single lens model from the slicing program. MLAs, microlens arrays.

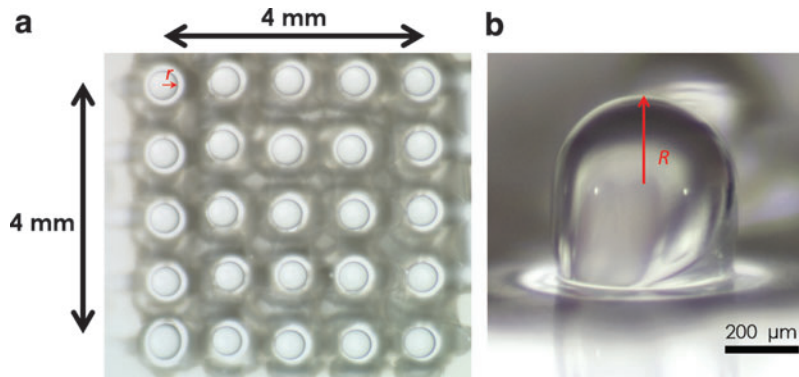


FIG. 2. Top view (a) of the  $5 \times 5$  MLA, and side view (b) of a single micro-lens.

for printing the MLA as well as for postprocessing. The printer used multiple beams from a  $\text{CO}_2$  laser to locally heat and soften/melt the substrate and glass filament. The  $\text{CO}_2$  laser operated at a wavelength of  $10.6 \mu\text{m}$ .

The technique is similar to the one, demonstrated previously by Kinzel et al.<sup>20–23</sup> The current 3D printer, however, uses four symmetrically placed beams surrounding the glass filament, which was fed perpendicular to the fused quartz plate. Before printing, the protective coating was removed from the filament using mechanical stripping pliers. A schematic of the print head is shown in Figure 1a, depicting the filament that was fed into the hot zone created by the laser beams. The filament was deposited onto the glass plate in a predetermined layer-by-layer geometry using a machine code, which was generated using a commercial slicing software such as Simplify3D or PrusaSlicer.

To test the printability of MLAs, a CAD model of a  $5 \times 5$  lens array was designed having a 1 mm center-to-center separation between lenses. In the CAD model, the radius of each micro-lens was designed to be  $300 \mu\text{m}$ . In Figure 1b, the sliced model of the MLA is shown with Figure 1c showing a single lens, indicating the two-layer structure of the print.

Fabrication of the  $5 \times 5$  MLA was performed with a print speed of 100 mm/min resulting in a total printing time of  $\sim 4$  min, that is,  $< 10$  s/lens. The laser power launched at the hot zone and filament by the four beams was estimated to be 7.5 W. During printing, the glass filament was fed into the hot zone and subsequently softened and fused to the glass substrate. Owing to the similar size of the hot zone and the micro-lens being printed, in combination with the relatively high laser power used, the printed glass was partially molten during deposition and, therefore, reshaped due to surface tension.

This unique effect resulted in fully dense glass micro-lenses without any voids or layer gaps. The final size and shape of a micro-lens is determined by several parameters, including the initial CAD model, slicing algorithm and printer settings (print speed and filament feed rate), filament diameter, and laser power settings and focused spot size of the laser beams. For producing size- and shape-specific micro-lens designs parameter mapping is required, for which the matrix printing ability of the glass 3D printer is highly suitable for. The high laser power used during printing caused a small amount of glass to be evaporated from the hot zone, with a subsequent partial redeposit of fumed silica surrounding the micro-lens and, in some instances, onto nearby micro-lenses.

To remove this unwanted redeposited material, each lens was irradiated using the  $\text{CO}_2$  laser for a duration of  $\sim 10$  s, using the four laser beams with a total power of 5 W. Figure 2a shows the printed and postprocessed MLA. The redeposited fumed silica can be seen here as darker regions between the micro-lenses. Figure 2b shows a close-up of a single lens from the same MLA, corresponding to the sliced model in Figure 1c.

Fabrication of micro-lenses with different heights was possible simply by varying the number of print layers. Figure 3 shows images of three different micro-lenses, having a similar convex radius but different thickness, printed with a single layer (shown in Fig. 3a), double layer (Fig. 3b), and five layers (shown in Fig. 3c). Note that within the five-layer micro-lens, some small voids are visible that likely are formed during layer shifting. Further improvement of the process parameters is needed for printing multilayer MLA ( $\geq 5$  layers).

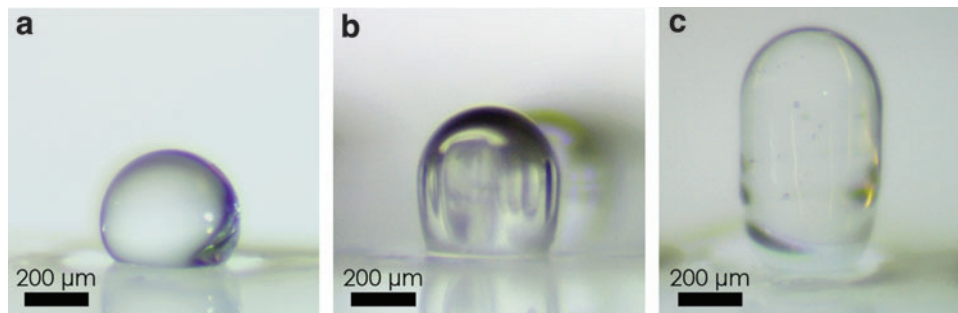


FIG. 3. Micro-lenses in different thickness: (a) 1-layer micro-lens, (b) 2-layer micro-lens, (c) 5-layer micro-lens.

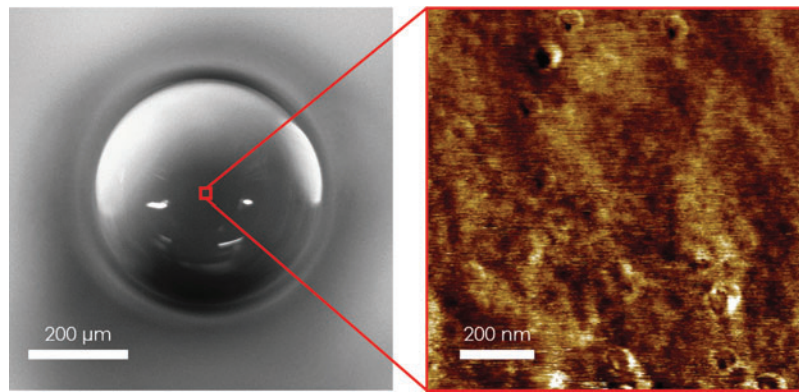


FIG. 4. Roughness measurement by AFM on an example microlens. AFM, atomic force microscopy.

### Characterization

To evaluate the reproducibility of the 3D printing technique, the MLA was characterized using optical microscopy (Nikon Eclipse LV100) in combination with image processing (ImageJ). The surface roughness was measured for several microlenses using atomic force microscopy (Bruker Dimension ICON). The optical properties of the lenses were measured and compared with the lens maker's formula as well as the ray optics model using COMSOL simulations.

#### Optical microscopy

The plano-convex shape of the printed microlenses, shown in Figure 2, was characterized using an optical microscope in combination with image processing. As an example, the single lens shown in Figure 2b has a radius of curvature,  $R$ , of the convex face equal to  $R = 232 \mu\text{m}$ . The distance from the substrate plane to the lens vertex was measured to be  $472 \mu\text{m}$ .

The measured radius from the top view (shown in Fig. 2a),  $r$ , of the lens was  $232 \mu\text{m}$ . The similar values of the radius of curvature ( $R$ ) to the cross-section radius ( $r$ ) suggests that the convex microlens was nearly hemispherical in shape. The standard deviation for the cross-section radius ( $r$ ) of all the lenses in the MLA was 1.3% ( $232 \pm 3 \mu\text{m}$ ).

There is a slight misalignment of the lenses along rows/columns as seen in the MLA shown in Figure 2a. This misalignment was believed to have been influenced by hysteresis of the 3D translation stage of the printer. However, the main cause is ascribed to the slicing program that outputs a machine code with slightly variable starting coordinates for each lens position (can be observed in Fig. 1b), that is, first contact point between filament and glass substrate. Owing to wetting of the glass to the substrate, in combination with surface tension of the molten glass, the center position of each lens is slightly shifted and does not strictly follow coordinates of the CAD model.

#### Surface roughness

The surface roughness for several microlenses was characterized using atomic force microscopy. A typical measurement performed near the apex of the lens is shown in Figure 4, indicating the average surface roughness of  $R_a = 0.12 \text{ nm}$ , exceeding the microlens surface roughness of  $6 \text{ nm}$  in the aforementioned studies.<sup>29,30,32,33</sup> For context, a dual-axis wheel polished glass typically has a surface roughness of  $1.24 \text{ nm}$ .<sup>34</sup>

#### Optical (lens) properties

The effective focal length (EFL),  $f$ , for a plano-convex lens with respect to the principal planes can be estimated by an equation derived from lens maker's formula:

$$\frac{1}{f} = \frac{(n-1)}{R}, \quad (1)$$

where  $n$  is the refractive index of fused silica ( $n = 1.459$ , at  $\lambda = 0.588 \mu\text{m}$ ). The estimated EFL of the single microlens, shown in Figure 2b, is  $f = 505 \mu\text{m}$ , which refers to the back focal length (BFL) from the lens vertex for a plano-convex configuration.

For light propagation in the opposite direction, the lens is in a convex-plano shape, which has the same EFL as the

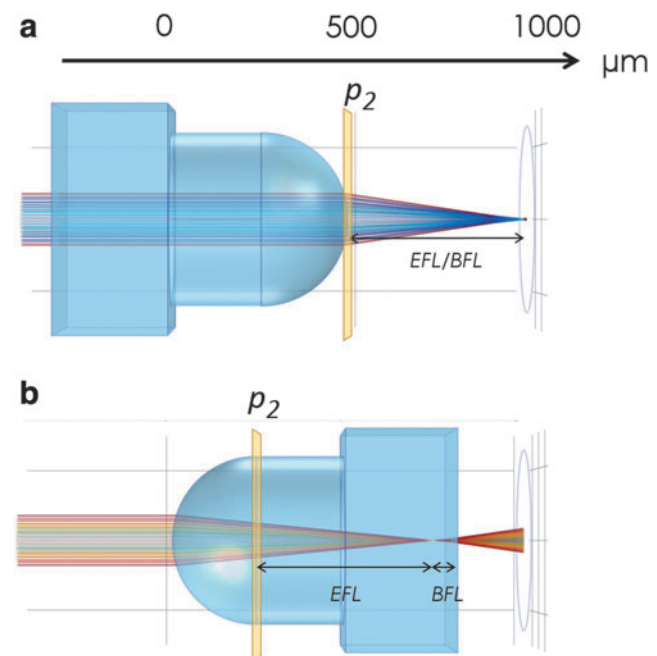


FIG. 5. Simulations of the focusing performance of the microlens. The model included the quartz glass substrate (the square volume), which has the same refractive index as the microlens (a) plano-convex configuration, (b) convex-plano configuration.

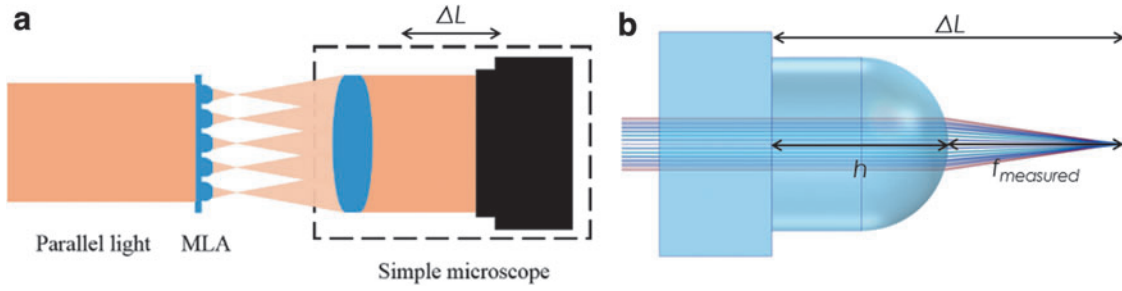


FIG. 6. The schematic (a) of the optical setup for focal length measurement, with definitions shown in (b).

plano-convex lens. The BFL can be estimated by subtracting the secondary principle plane position,  $p_2$ , from the EFL,  $f$ . The position of the secondary principle plane can then be calculated using the equation:

$$p_2 = -\frac{f(n-1)t}{nR}, \quad (2)$$

where  $t$  is the lens thickness, which in this case is  $772 \mu\text{m}$  (lens height  $472 \mu\text{m}$  + substrate thickness  $300 \mu\text{m}$ ). BFL for convex-plano configuration is thus estimated to be  $-24 \mu\text{m}$  suggesting the focal point is  $24 \mu\text{m}$  below the plano surface, within the silica glass substrate.

Simulations of the parallel ray propagation (at  $\lambda = 0.588 \mu\text{m}$ ) through the single microlens were performed for both plano-convex and convex-plano directions using a COMSOL ray optics model. The results are shown in Figure 5. The simulated BFL is  $475 \mu\text{m}$  for the plano-convex configuration and  $-36 \mu\text{m}$  for the convex-plano configuration, respectively.

The optical focal length of the microlenses was further measured by using the setup depicted in Figure 6a, with Figure 6b showing the relevant parameters. Here a simple optical microscope was constructed using an objective lens and a CCD camera at a fixed distance. A parallel white light beam was projected through and focused by the glass MLA. Initially, a clear image was captured of the substrate surface by adjusting the microscope position relative to the MLA. The microscope position was then changed until the image plane overlapped with the optimum MLA focal plane where most focal spots were minimized. A spot-matrix image captured at this position is shown in Figure 6a.

The focal length ( $f_{\text{measured}} = 483 \pm 40 \mu\text{m}$ ) was obtained by subtracting the average lens height ( $475 \pm 5 \mu\text{m}$ ) from the measured distance  $\Delta L$  between the two microscope positions ( $958 \pm 40 \mu\text{m}$ ). The homogeneity of the spots was then analyzed by comparing the intensity of the spots along a selected array of spots. The light intensity of the selected array with five spots (indicated by the red box in Fig. 7a) was measured with the results presented in Figure 7b. The intensities were measured across the center of each spot and quantified using image processing software ImageJ. The result from the five selected microlenses shows uniform light intensities for the different lenses with a variation of  $\pm 3.4\%$ , indicating similar focusing performance for each microlens in the glass MLA.

#### Imaging performance

The imaging performance of the microlens was also evaluated as shown in Figure 8. Here a parallel white light source was projected through a filter (black Swedish Dala horse on a white paper), through the MLA with the image captured using the CCD camera of the optical microscope. Each lens provides a clear image with little distortion (see Fig. 8b) indicating reproducible fabrication and homogeneous refractive index of the different lenses with overall good imaging performance of the MLA.

#### Conclusions

We present results on a simple and rapid method of 3D printing silica glass MLA using a filament-based laser deposition technology. The microlenses had a hemispherical

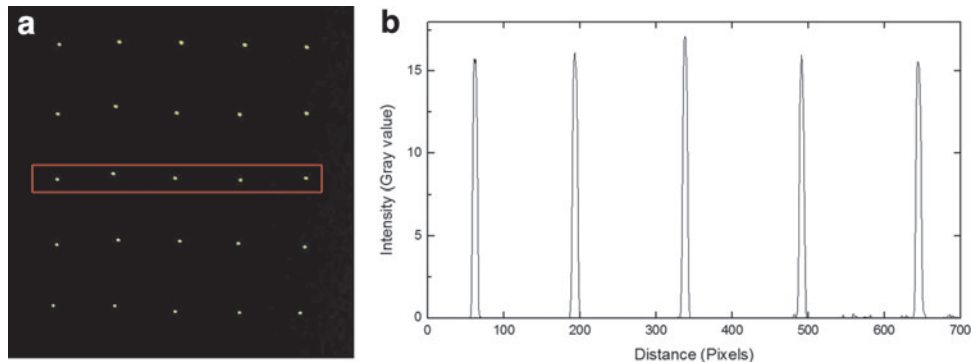


FIG. 7. (a) Spot-matrix image captured from the focal plane of the MLA, (b) light intensities of five spots taken from the red box area.

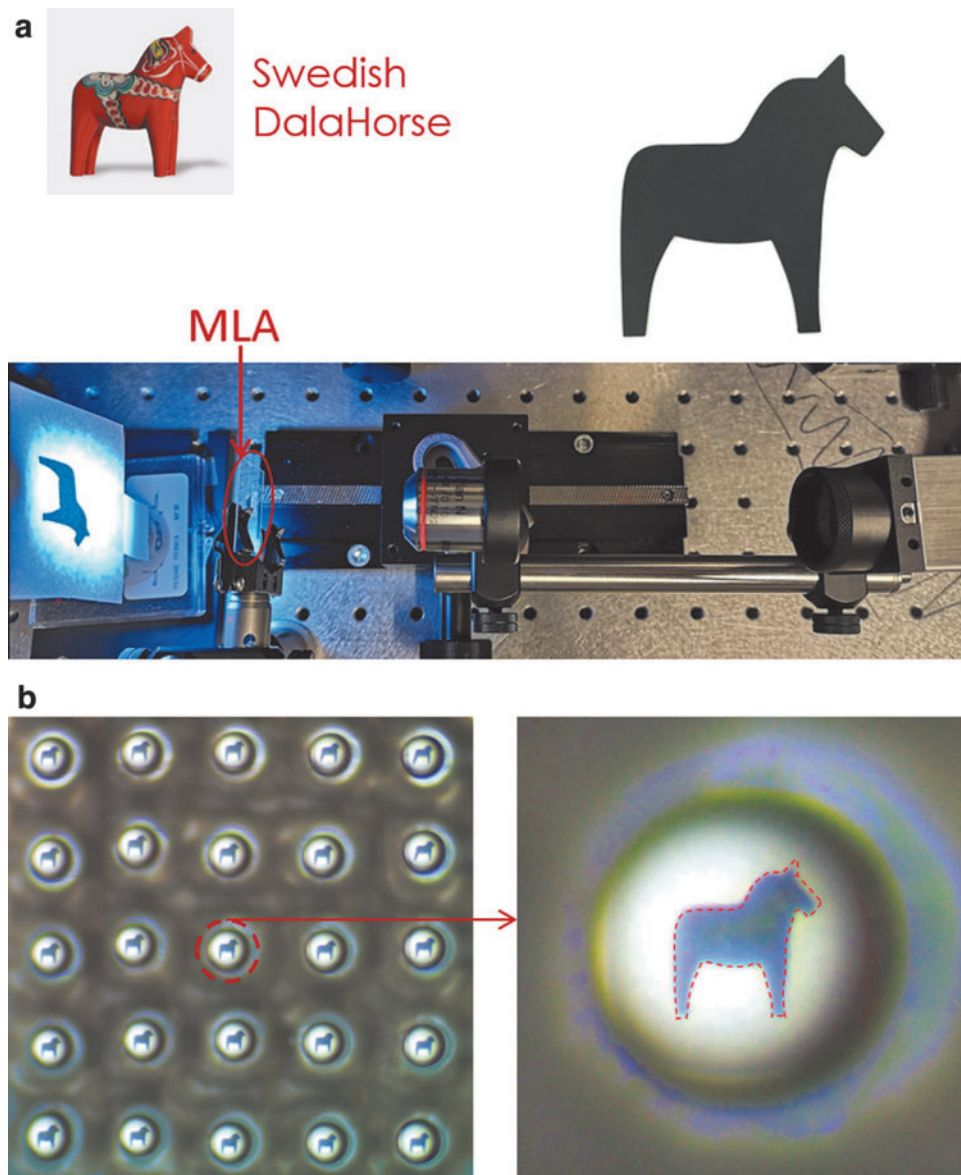


FIG. 8. (a) The setup for the MLA imaging performance test, (b) the *top view* of the  $5 \times 5$  MLA imaging of a Swedish Dala horse and the comparison of a lens imaging with the original image outline (*red dashed outline*).

plano-convex shape. An ultrasmooth lens surface was achieved with a measured roughness of 0.12 nm. The  $5 \times 5$  MLA displays uniform focusing performance with an average EFL of  $483 \pm 40 \mu\text{m}$  across the whole array, in agreement with theoretical values and simulation results. The MLA provides good imaging quality. The capability of creating microlenses in different thickness enables versatile customizations of microlenses and multifocal MLA fabrications for 3D imaging applications.

#### Authors' Contributions

Conceptualization, methodology, validation, investigation, visualization, and writing—original draft by C.L. Visualization and writing—reviewing and editing by T.O. Investigation by C.L. Writing—reviewing and editing by C.M.H. Supervision, methodology, and writing—reviewing and editing by M.F.

#### Author Disclosure Statement

Nobula3D AB is a spin-off company from the project RMA15-0135, funded by the Swedish Foundation for Strategic Research. No competing financial interests or conflict of interests exist.

#### Funding Information

We acknowledge funding from the Swedish Foundation for Strategic Research (Grant No. RMA15-0135).

#### References

1. Yuan W, Li L-H, Lee W-B, et al. Fabrication of microlens array and its application: A review. *Chin J Mech Eng* 2018;31(1):16; doi: 10.1186/s10033-018-0204-y
2. Bardinal V, Daran E, Leichlé T, et al. Fabrication and characterization of microlens arrays using a Cantilever-

- Based Spotter. *Opt Express* 2007;15(11):6900; doi: 10.1364/OE.15.006900
3. Li Y, Li K, Gong F. Fabrication and optical characterization of polymeric aspherical microlens array using hot embossing technology. *Appl Sci* 2021;11(2):882; doi: 10.3390/app11020882
  4. Ottevaere H, Cox R, Herzig HP, et al. Comparing glass and plastic refractive microlenses fabricated with different technologies. *J Opt Pure Appl Opt* 2006;8(7):S407–S429; doi: 10.1088/1464-4258/8/7/S18
  5. Huang C-Y, Hsiao W-T, Huang K-C, et al. Fabrication of a double-sided micro-lens array by a Glass Molding Technique. *J Micromechanics Microengineering* 2011;21(8):085020; doi: 10.1088/0960-1317/21/8/085020
  6. Li K, Huang X, Chen Q, et al. Flexible fabrication of optical glass micro-lens array by using contactless hot embossing process. *J Manuf Process* 2020;57:469–476; doi: 10.1016/j.jmapro.2020.07.019
  7. Kim HM, Kim MS, Lee GJ, et al. Large area fabrication of engineered microlens array with low sag height for light-field imaging. *Opt Express* 2019;27(4):4435; doi: 10.1364/OE.27.004435
  8. Oh H, Kim G, Seo H, et al. Fabrication of micro-lens array using quartz wet etching and polymer. *Sens Actuators Phys* 2010;164(1–2):161–167; doi: 10.1016/j.sna.2010.10.003
  9. Nussbaum P, Völkel R, Herzig HP, et al. Design, fabrication and testing of microlens arrays for sensors and microsystems. *Pure Appl Opt J Eur Opt Soc Part A* 1997;6(6):617–636; doi: 10.1088/0963-9659/6/6/004
  10. Haselbeck S. Microlenses fabricated by melting a photoresist on a base layer. *Opt Eng* 1993;32(6):1322; doi: 10.1117/12.135845
  11. Stern MB, Rubico Jay T. Dry etching for coherent refractive microlens arrays. *Opt Eng* 1994;33(11):3547–3551; doi: 10.1117/12.179880
  12. He M, Yuan X-C, Ngo NQ, et al. Single-step fabrication of a microlens array in sol–gel material by direct laser writing and its application in optical coupling. *J Opt Pure Appl Opt* 2004;6(1):94–97; doi: 10.1088/1464-4258/6/1/017
  13. Wakaki M, Komachi Y, Kanai G. Microlenses and microlens arrays formed on a glass plate by use of a CO<sub>2</sub> laser. *Appl Opt* 1998;37(4):627; doi: 10.1364/AO.37.000627
  14. Sohn I-B, Yoo D, Noh Y-C, et al. Formation of a plano-convex micro-lens array in fused silica glass by using a CO<sub>2</sub> laser-assisted reshaping technique. *J Korean Phys Soc* 2016;69(3):335–343; doi: 10.3938/jkps.69.335
  15. Choi H-K, Ahsan MdS, Yoo D, et al. Formation of cylindrical micro-lens array on fused silica glass surface using CO<sub>2</sub> laser assisted reshaping technique. *Opt Laser Technol* 2015;75:63–70; doi: 10.1016/j.optlastec.2015.05.022
  16. Sohn I-B, Choi H-K, Noh Y-C, et al. Laser assisted fabrication of micro-lens array and characterization of their beam shaping property. *Appl Surf Sci* 2019;479:375–385; doi: 10.1016/j.apsusc.2019.02.083
  17. Kostyuk GK, Zakoldaev RA, Sergeev MM, et al. Microlens array fabrication on fused silica influenced by NIR laser. *Appl Phys B* 2016;122(4):99; doi: 10.1007/s00340-016-6379-y
  18. Zakoldaev RA, Kostyuk GK, Koval VV, et al. Microlens array fabrication on fused silica by LIBBH Technology with CO<sub>2</sub> Laser Smoothing. *Izv Vysš Učebn Zaved Priborostr* 2016;59(5):400–406; doi: 10.17586/0021-3454-2016-59-5-400-406
  19. Chao H, Furong L, Weiping Z, et al. Fabrication of microtransmittance grating using laser induced backside dry etching. *J Laser Appl* 2012;24(1):012001; doi: 10.2351/1.3656488
  20. Sleiman K, Rettschlag K, Jäschke P, et al. Material loss analysis in glass additive manufacturing by laser glass deposition. *J Laser Appl* 2021;33(4):042050; doi: 10.2351/7.0000482
  21. Hostetler JM, Goldstein JT, Bristow D, et al. Fiber-fed laser-heated process for printing transparent glass from single mode optical fiber. In: *Proceedings of SPIE 10523, Laser 3D Manufacturing V*; San Francisco, United States: SPIE LASE, 2018; doi: 10.1117/12.2291443
  22. Luo J, Hostetler JM, Gilbert L, et al. Additive manufacturing of transparent fused quartz. *Opt Eng* 2018;57(04):1; doi: 10.1117/1.OE.57.4.041408
  23. Hostetler JM, Johnson JE, Goldstein JT, et al. Fiber-Fed Printing of Free-Form Free-Standing Glass Structures. In: *Proceedings of SFF Symposium*; Austin, Texas: Solid Freeform Fabrication Symposium, 2018; pp. 994–1002; doi: 10.1117/12.2510345
  24. Moore DG, Barbera L, Masania K, et al. Three-dimensional printing of multicomponent glasses using phase-separating resins. *Nat Mater* 2020;19(2):212–217; doi: 10.1038/s41563-019-0525-y
  25. Klein J, Stern M, Franchin G, et al. Additive manufacturing of optically transparent glass. *3D Print Addit Manuf* 2015;2(3):92–105; doi: 10.1089/3dp.2015.0021
  26. Inamura C, Stern M, Lizardo D, et al. Additive manufacturing of transparent glass structures. *3D Print Addit Manuf* 2018;5(4):269–283; doi: 10.1089/3dp.2018.0157
  27. Maniewski P, Laurell F, Fokine M. Laser cladding of transparent fused silica glass using Sub-Mm Powder. *Opt Mater Express* 2021;11(9):3056; doi: 10.1364/OME.433734
  28. Comesaña R, Quintero F, Lusquinos F, et al. Laser cladding of bioactive glass coatings. *Acta Biomater* 2010;6(3):953–961; doi: 10.1016/j.actbio.2009.08.010
  29. Kotz F, Quick AS, Risch P, et al. Two-photon polymerization of nanocomposites for the fabrication of transparent fused silica glass microstructures. *Adv Mater* 2021; 33(9):2006341; doi: 10.1002/adma.202006341
  30. Hong Z, Ye P, Loy DA, et al. Three-dimensional printing of glass micro-optics. *Optica* 2021;8(6):904–910; doi: 10.1364/OPTICA.422955
  31. Mader M, Hambitzer L, Schlautmann P, et al. Melt-extrusion-based additive manufacturing of transparent fused silica glass. *Adv Sci* 2021;8(23):2103180; doi: 10.1002/adv.202103180
  32. Kotz F, Arnold K, Bauer W, et al. Three-dimensional printing of transparent fused silica glass. *Nature* 2017;544(7650):337–339; doi: 10.1038/nature22061
  33. Toombs JT, Luitz M, Cook CC, et al. Volumetric additive manufacturing of silica glass with microscale computed axial lithography. *Science* 2022;376(6590):308–312; doi: 10.1126/science.abm6459
  34. Lu A, Jin T, Liu Q, et al. Modeling and prediction of surface topography and surface roughness in dual-axis wheel polishing of optical glass. *Int J Mach Tools Manuf* 2019;137:13–29; doi: 10.1016/j.ijmactools.2018.10.001

Address correspondence to:

Chunxin Liu  
 Department of Applied Physics  
 KTH Royal Institute of Technology  
 Stockholm 114 21  
 Sweden

E-mail: chunxin@kth.se